

**International Journal of Design Engineering**

ISSN online: 1751-5882 - ISSN print: 1751-5874

<https://www.inderscience.com/ijde>

---

**Lubricant distribution evolution in asymmetric double-row tapered roller bearings during the loss of lubrication process**

Xueqiang Bai, Fengxia Lu, Mou Li, Wenlin Zhu, Rupeng Zhu

**DOI:** [10.1504/IJDE.2023.10057307](https://doi.org/10.1504/IJDE.2023.10057307)

**Article History:**

Received:	07 September 2021
Last revised:	12 August 2022
Accepted:	31 August 2022
Published online:	05 July 2023

---

## **Lubricant distribution evolution in asymmetric double-row tapered roller bearings during the loss of lubrication process**

---

Xueqiang Bai, Fengxia Lu\* and Mou Li

National Key Laboratory of Science  
and Technology on Helicopter Transmission,  
Nanjing University of Aeronautics and Astronautics,  
29 Yudao St., Jiangsu Province, Nanjing, 210000, China  
Email: baixueqiang@nuaa.edu.cn  
Email: meefxlu@nuaa.edu.cn  
Email: lmchanic@nuaa.edu.cn  
\*Corresponding author

Wenlin Zhu

National Key Laboratory of Science  
and Technology on Helicopter Transmission,  
Nanjing University of Aeronautics and Astronautics,  
29 Yudao St., Jiangsu Province, Nanjing, 210000, China  
and  
National Key Laboratory of Science  
and Technology on Helicopter Transmission,  
AECC Hunan Aviation Powerplant Research Institute,  
Zhuzhou, China  
Email: zhuwenlin0610@163.com

Rupeng Zhu

National Key Laboratory of Science  
and Technology on Helicopter Transmission,  
Nanjing University of Aeronautics and Astronautics,  
29 Yudao St., Jiangsu Province, Nanjing, 210000, China  
Email: rpzhu\_nuaa@163.com

**Abstract:** Double row tapered roller bearings have excellent load-carrying behaviour and are widely used in helicopter tail drive systems. If the helicopter is attacked, the bearings are working at loss of lubrication condition. This study using the R10 method to discretise the amount of oil to explore the evolution of lubricating oil distribution in the support bearing of a helicopter tail drive system under lubrication loss conditions based on the idea of computational fluid dynamics (CFD) and considers the revolution and rotation speed of bearings. The lubricant distribution on the large rollers, small rollers, and inner ring walls on both asymmetrical sides was analysed, and the quantity of oil and lubricant inside the bearing were estimated. It is found that the recommended

speed range of bearing is 4,000–5,000 r/min, and the value for the number of rollers in the bearing was determined to be no more than 22 large rollers and no more than 25 small rollers.

**Keywords:** asymmetric; double-row tapered roller bearing; loss of lubrication; lubricant distribution; rotation; computational fluid dynamics; CFD.

**Reference** to this paper should be made as follows: Bai, X., Lu, F., Li, M., Zhu, W. and Zhu, R. (2023) ‘Lubricant distribution evolution in asymmetric double-row tapered roller bearings during the loss of lubrication process’, *Int. J. Design Engineering*, Vol. 12, No. 1, pp.49–68.

**Biographical notes:** Xueqiang Bai received a Master’s degree in Mechanical Engineering from Nanjing University of Aeronautics and Astronautics. During the period of his master degree study, he was mainly engaged in the research of bearing friction and lubrication.

Fengxia Lu is a Doctor at the College of Mechanical and Electrical Engineering, Nanjing University of Aeronautics and Astronautics in Nanjing, China. She obtained her PhD in Mechanical Engineering from Nanjing University of Aeronautics and Astronautics. Her research interests include mechanical transmission, lubrication systems, and heat transfer.

Mou Li received a Master’s degree in Mechanical Engineering from Nanjing University of Aeronautics and Astronautics. During the period of his master degree study, he was mainly engaged in the study of heat-flow coupling of helicopter transmission system during the process of loss of lubrication.

Wenlin Zhu received a Master’s degree in Mechanical Engineering from Nanjing University of Aeronautics and Astronautics, and is currently studying for a PhD at Nanjing University of Aeronautics and Astronautics, while mainly engaged in the research of lubrication, heat transfer and structural optimisation of helicopter transmission systems.

Rupeng Zhu received his PhD in Engineering from Nanjing University of Aeronautics and Astronautics. Currently, he is mainly engaged in the professional construction and teaching of mechanical engineering, and the research on helicopter transmission.

---

## 1 Introduction

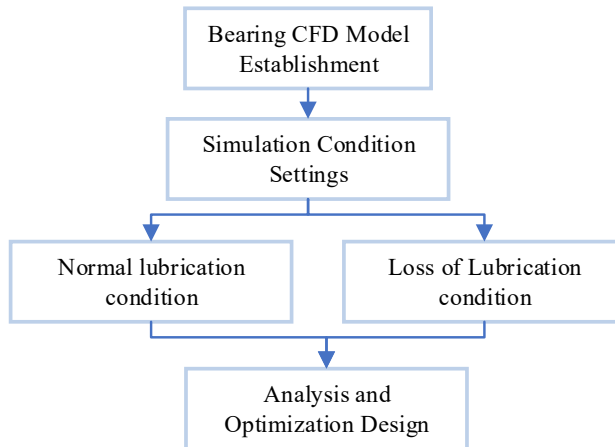
Double-row tapered roller bearings can withstand large radial and axial loads, and they are widely used in the tail horizontal shaft and tail tilt shafts of helicopters. During operation, the bearing is subjected to severe working conditions. If the lubrication system fails or is attacked, the amount of oil will continue to decrease, causing the bearing to fail. Thus, the bearing must have good lubrication in the case of loss of lubrication.

Currently, the computational fluid dynamics (CFD) method is widely used in the simulation analysis of bearing lubrication. Wenwei et al. (2009) established a simple CFD fluid domain model, using the Eulerian multiphase flow model and the re-normalisation group (RNG)  $k$ - $\epsilon$  turbulence model, according to different bearing speeds, lubricating medium speeds, gas contents, injection angles, and other working

conditions. Raju et al. (2013) used the reference frame method to simulate the motion of a bearing and studied the influence of different lubricating oil inlets on the lubrication of the bearing. Crouchez-Pillot and Morvan (2014) used the VOF method and grid-adaptive technology to track the oil and gas phases of the bearing cavity. Bristot et al. (2016) conducted a transient analysis of aero-engine bearings. Several previous studies used a sliding grid to simulate the rotation of the bearing while ignoring the rotation of the rolling elements, and studied the oil-gas two-phase flow in an oil-jet lubricated high-speed bearing (Guo et al., 2012; Hu et al., 2014; Wu et al., 2016a, 2016b; Yan et al., 2017; Zhai et al., 2014; Zhang et al., 2015). Yan et al. (2016a, 2016b) used a multiple coordinate system method and a two-phase flow model to analyse the influence of bearing revolution, steel ball spin, cage structure, and sealing conditions on bearing lubrication performance. Yan et al. (2016b) used a dynamic grid method to simulate and analyse the internal flow field of a bearing.

For ball bearings, Li et al. (2018) studied the effect of inlet air flow on the oil and gas distribution in the bearing cavity and the operating conditions of the bearing. Liu et al. (2018) studied the influence of local vortices in the bearing cavity on oil flow and analysed the speed and injection angle of the oil distribution in the bearing cavity. Liang et al. (2020) experimentally explored the effects of oil supply speed, viscosity, and other physical characteristics of oil on the distribution and return air near the bearing contact area through experiments. Peterson et al. (2021) found that grooves in the inner ring of angular contact ball bearings improved lubrication. Concli et al. (2020) used cylindrical roller bearings with different structures as the research object and studied the lubricating oil distribution in the bearing cavity and the power loss of the roller churning oil. Zhang (2018) established a CFD calculation model for tapered roller bearings that considered the rotation of the rolling elements and conducted a simulation study on the internal fluid domain of tapered roller bearings at different speeds, fuel injection levels, and numbers of nozzles.

**Figure 1** Structure of the article (see online version for colours)



Although CFD technology has been widely used in the calculation of oil distribution in bearing flow field and there are many simulation analyses of oil distribution in the bearing drainage area under full lubrication, there are few analyses on the continuous

change in lubricating oil during the loss of lubrication process. In this study, a CFD calculation model that reflects the special structure of the bearing and the real state of motion was established. By discretising the amount of inlet oil in the loss of lubrication process, the oil distribution law in the bearing flow field during this process is analysed. The influence of operating conditions and structural parameters on the lubricant distribution in the bearing flow field is analysed, and the optimal value of the number of rollers of the double-row tapered roller bearing is determined. And the structure of the article is shown in Figure 1.

## **2 CFD calculation model of double-row tapered roller bearings**

### *2.1 Calculation model*

The double-row tapered roller bearing in the helicopter tail drive system bears different loads on both sides of the rollers, so the number of rollers on each side is different. The outer ring rib structure is shown in Figure 2. During operation, the lubricating oil is stirred by the spiral bevel gear and is guided to the bearing through the oil guide tube of the middle reducer for bearing lubrication and cooling.

When the CFD method is used for simulation, the transition circle, chamfer, and other structures of the bearing increase the number of grids and the required calculation time. Therefore, to improve the quality of the grid and reduce the number of grids without affecting the calculation accuracy, we ignore the small structures that have little effect on the calculation result. Because the material and speed of the inner rings on the left and right sides of the double-row tapered roller bearing are the same, the two inner rings can be combined. Considering the meshing requirements of the bearing flow field, the rollers are reduced by 0.5 mm (Concli et al., 2020).

Because the size and number of rollers on both sides of the double-row tapered roller bearing are different, the computational domain is set to two areas, as shown in Figure 3.

### *2.2 Meshing*

A tetrahedral grid was used to mesh the bearing flow field. To ensure calculation accuracy and facilitate convergence, the mesh of the roller wall was locally encrypted to ensure there are at least two layers of grids between the roller and the raceway wall, as shown in Figure 4. Because of the large turbulent kinetic energy at the oil inlet, this area is also locally refined, as shown in Figure 5.

To eliminate the influence of mesh density on the calculation results for the lubricating oil distribution, a mesh independence verification is required. Taking the volume fraction of lubricating oil on the roller wall as a physical quantity, the calculation results are shown in Figure 6. It can be seen that when the number of grids reaches 1,745,969, and it continues to increase, the change trend in the volume fraction of the lubricant on the roller wall slows. However, as the number of grids increases, the calculation time increases as well. Therefore, the final number of grids was determined to be 1,745,969.

**Figure 2** Double-row tapered roller bearing, (a) bearing structure, (b) bearing position

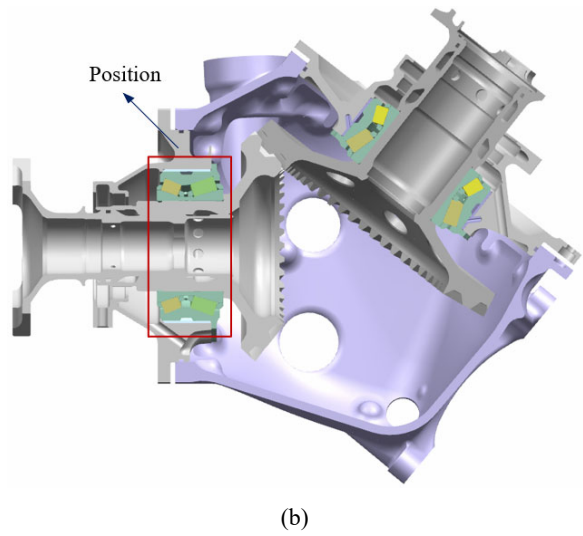
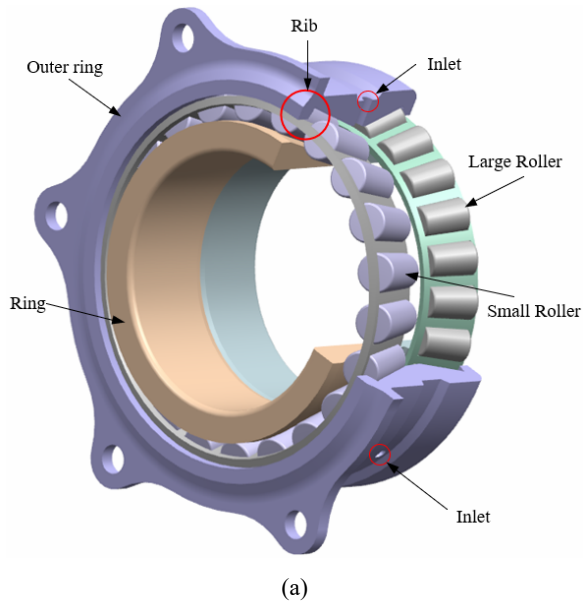


**Figure 3** Bearing flow field used in the simulations (see online version for colours)

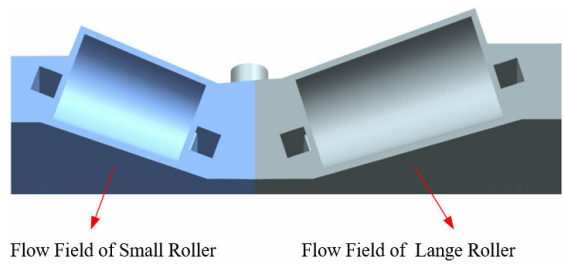


**Figure 4** Mesh of the roller wall (see online version for colours)

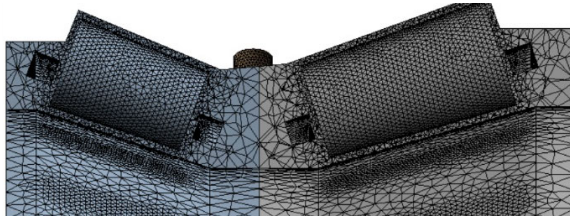


**Figure 5** Grids at the inlet (see online version for colours)

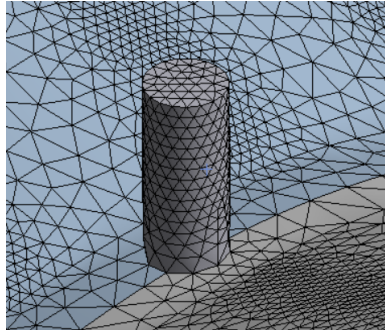
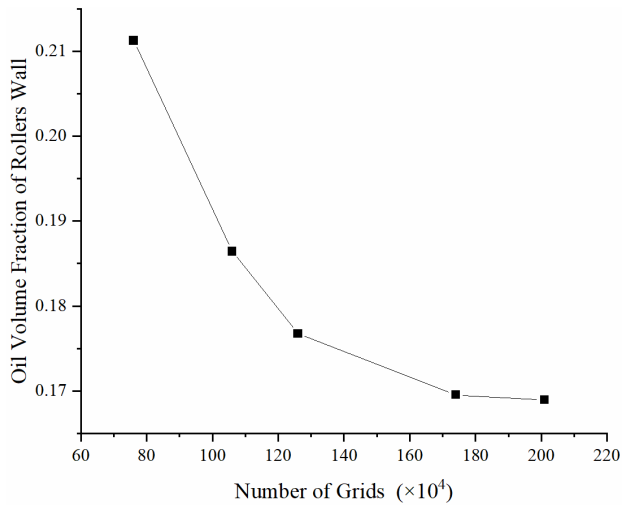


**Figure 6** Grid independence verification



### 3 CFD theory and simulation settings

#### 3.1 Multiphase flow model

This study uses the VOF model, which can solve complex flow problems, to simulate the clear interphase interface of multiphase flow. The sum of the volume fractions of all phases in each control volume in the model was unity.

$$\varphi_{air} + \varphi_{oil} = 1 \tag{1}$$

where  $\varphi_{oil}$  represents the density of the lubricating oil and  $\varphi_{air}$  represents the velocity vector.

#### 3.2 Boundary condition setting

The lubricating oil enters the bearing flow area through the two oil inlets above the bearing, which was set as the mass flow inlet. The inlet oil mass was set to 0.02 kg/s; both sides of the bearing basin and the other four oil injection ports were set as the pressure outlet, and the outlet pressure was zero.

Considering the revolution and rotation of the bearing, the watersheds on both sides were set as rotating areas, and the speed of the rotating area was determined by equations (2) and (3). The outer ring wall was set as a fixed wall, the inner ring wall was set as a rotating wall, and the rotation speed was 5,000 r/min.

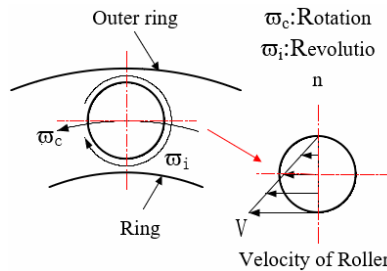
$$n_c = \frac{n(1-\gamma_i)}{2} \tag{2}$$

$$\gamma_i = \frac{D_i \cos \alpha_i}{d_{m,i}} \tag{3}$$

where  $n_c$  is the revolution speed of the roller,  $n$  is the input speed,  $D_i$  is the average diameter of the roller,  $d_{m,i}$  is the pitch circle diameter,  $\alpha_i$  is the contact angle of the roller, and  $i = 1, 2$  represents two rows of rollers.

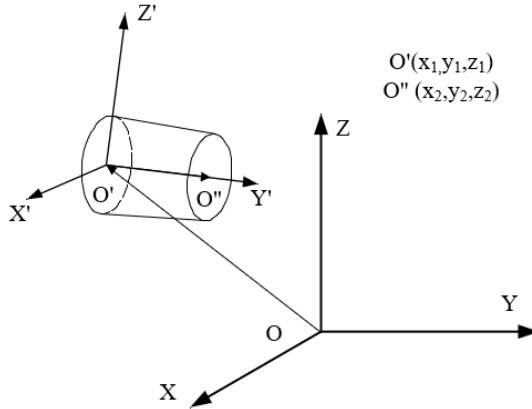
The roller motion was assumed to be the vector superposition of the revolution motion around the rotation axis and the rotation motion of the roller around its own axis. The gyroscopic motion of the roller and the sliding between the inner and outer ring walls was ignored. The roller was assumed to be purely rolling, as shown in Figure 7.

**Figure 7** Roller motion (see online version for colours)



The flow field on both sides of the bearing was set as the rotation area, and the rotation speed was the roller revolution speed; the roller wall was set as the rotating wall relative to the rotation area where it is located. The rotation centre and rotation vector of the roller are shown in Figure 8. The wall of the cage was set as a rotating wall.

**Figure 8** Roller position



To simulate the fluid flow on the curved wall as realistically as possible, the *RNG k-ε* model was selected, and the second-order upwind format was adopted. The SIMPLEC algorithm was used to improve the convergence speed while ensuring calculation accuracy.

#### 4 Prediction of lubricating oil distribution for double-row tapered roller bearings under fully lubricated conditions

##### 4.1 Prediction and analysis of bearing lubricating oil distribution under fully lubricated state

The large rollers along the rotating direction of the bearing are numbered; the roller under the oil inlet is number one. The volume fraction of oil on the roller wall at each position is shown in Figure 9. It can be seen that most of the lubricating oil adheres to the wall of the outer ring under the influence of centrifugal force. However, the area with the largest oil volume fraction on the outer ring wall is at the bottom-right corner.

To analyse this phenomenon, the lubricating oil at the cross section of the large roller was taken as the research object, as shown in Figure 10.

The oil droplets are comprehensively affected by the force  $F$  of the gas flowing inside the bearing and gravity  $G$ . A schematic of the force of the lubricating oil droplets on the large roller section is shown in Figure 11. At position 1, the oil droplet that just entered the bearing has an initial speed of  $V$  pointing to the inner ring of the bearing. Then, while the oil droplets are moving from position 1 to positions 2 and 3, the direction of the composition of forces acting on the oil droplets gradually changes and finally points to the outer ring. Affected by the resultant force, the speed direction of the oil droplets also changes, causing oil droplets to increasingly adhere to the outer ring during this process. Therefore, the oil between the roller and the wall of the inner ring near the inlet area is

sufficient, but the volume fraction of the oil between the roller and the wall of the outer ring is small. There is sufficient oil in the area between the lower roller and the outer ring in the bearing flow field; however, there is a small oil volume fraction between the roller and inner race. Thus, roller number 8 with abundant oil between the inner and outer ring walls is the roller with the best lubrication condition. This result shows the similar oil distribution in the bearing flow-field, compared with the research of Zhang et al. (2015).

**Figure 9** Oil distribution at the wall of the rollers (see online version for colours)

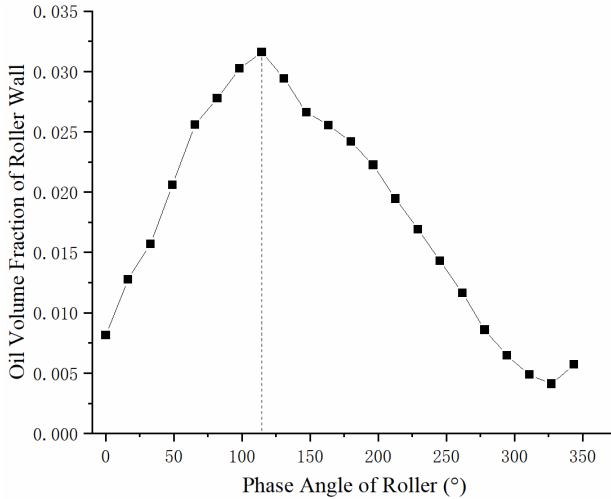
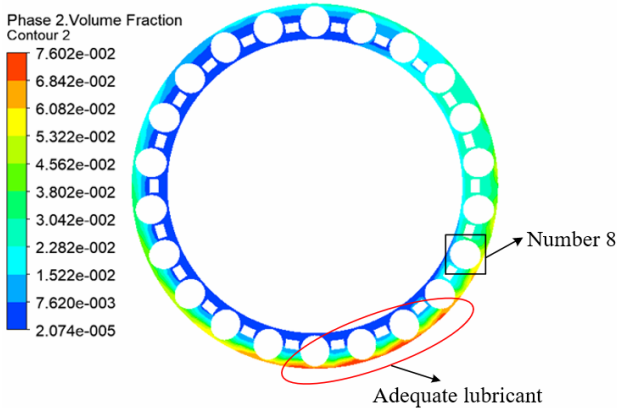


**Figure 10** Oil distribution at the cross section of the large roller (see online version for colours)



The oil distribution in the centre section of small roller number 7 was used as the research object, as shown in Figure 12. It can be seen that most of the lubricating oil flows out of the bearing cavity through the gap between the rollers and outer ring wall. During this process, the lubricating oil is blocked by the outer ring ribs and flows through the outer ring ribs, lubricating the big end of the bearing roller.

**Figure 11** Force acting upon oil droplets (see online version for colours)

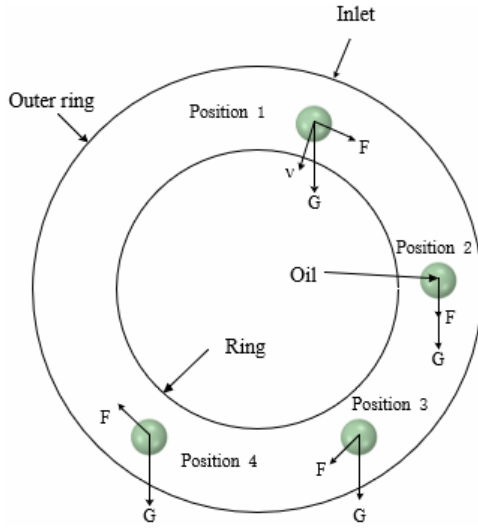
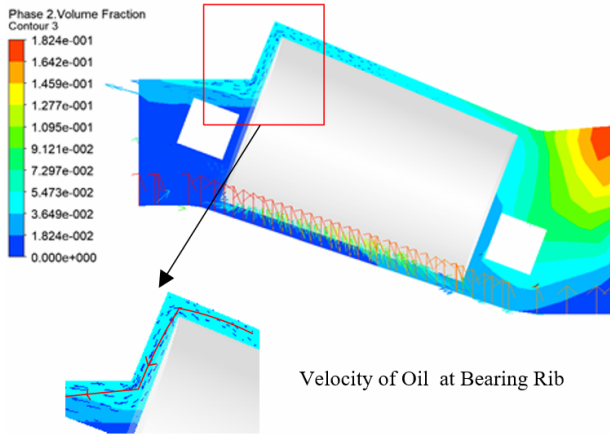


**Figure 12** Oil distribution at the centre section of small roller no. 7 (see online version for colours)



## 5 Changes in the lubricating oil distribution in the bearing basin during the loss of lubrication process

### 5.1 Discrete method of oil volume reduction

In the state of loss of lubrication, the lubricating oil provided by the helicopter reducer to the bearing is gradually reduced. The change of inlet oil mass was used to simulate this process. The inlet flow was discretised into 11 nodes according to the R10 priority coefficient method until the oil volume was reduced to zero. When the oil volume was

close to zero, the nodes are closer, which is convenient for observing whether the lubricating oil distribution in the bearing drainage area changes drastically.

**Figure 13** Change in oil distribution, (a)  $x = 0.016\text{kg/s}$ , (b)  $x = 0.0126\text{kg/s}$ , (c)  $x = 0.01\text{kg/s}$ , (d)  $x = 0.008\text{kg/s}$ , (e)  $x = 0.0063\text{kg/s}$ , (f)  $x = 0.005\text{kg/s}$ , (g)  $x = 0.004\text{kg/s}$ , (h)  $x = 0.0032\text{kg/s}$ , (i)  $x = 0.0025\text{kg/s}$ , (j)  $x = 0.002\text{kg/s}$  (see online version for colours)

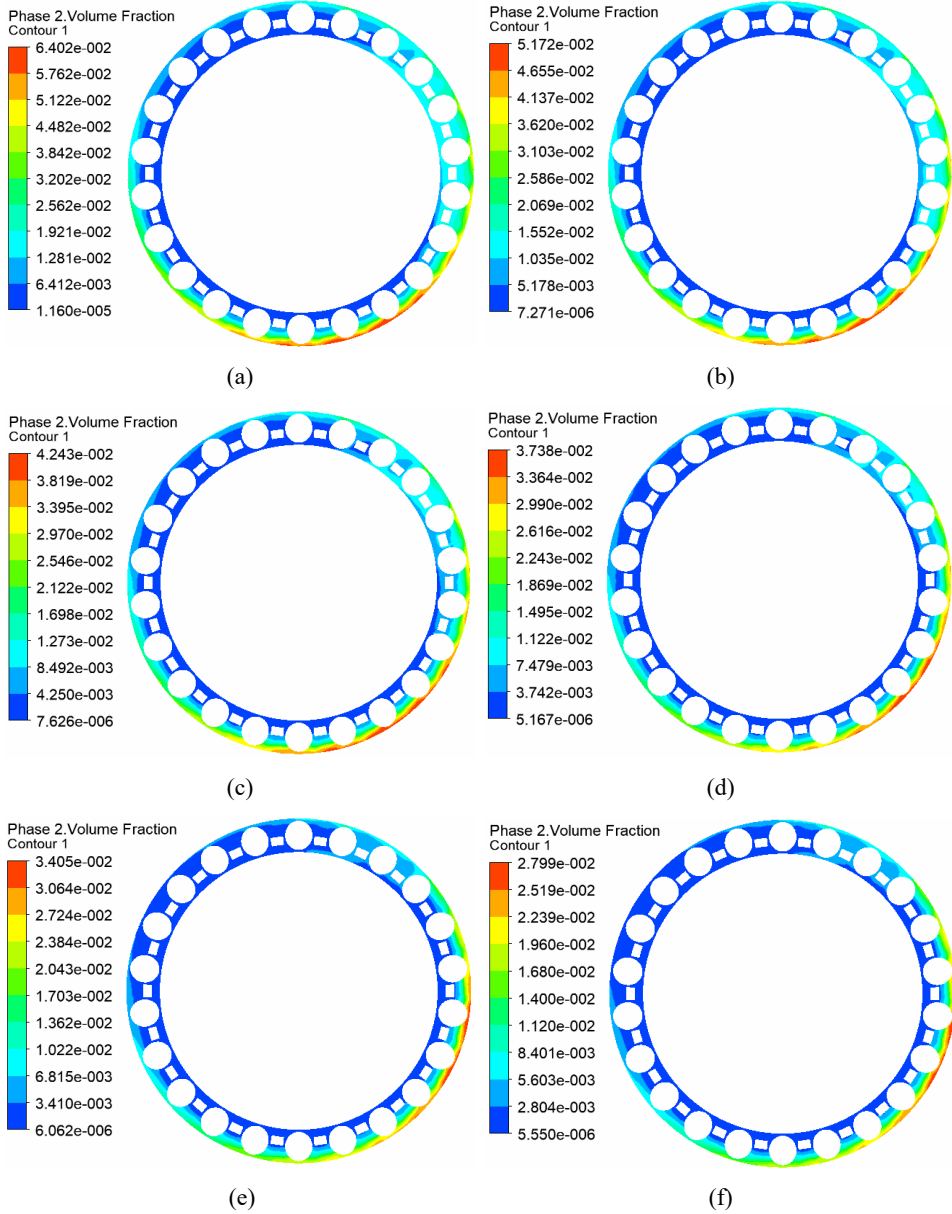


**Figure 13** Change in oil distribution, (a)  $x = 0.016\text{kg/s}$ , (b)  $x = 0.0126\text{kg/s}$ , (c)  $x = 0.01\text{kg/s}$ , (d)  $x = 0.008\text{kg/s}$ , (e)  $x = 0.0063\text{kg/s}$ , (f)  $x = 0.005\text{kg/s}$ , (g)  $x = 0.004\text{kg/s}$ , (h)  $x = 0.0032\text{kg/s}$ , (i)  $x = 0.0025\text{kg/s}$ , (j)  $x = 0.002\text{kg/s}$  (continued) (see online version for colours)

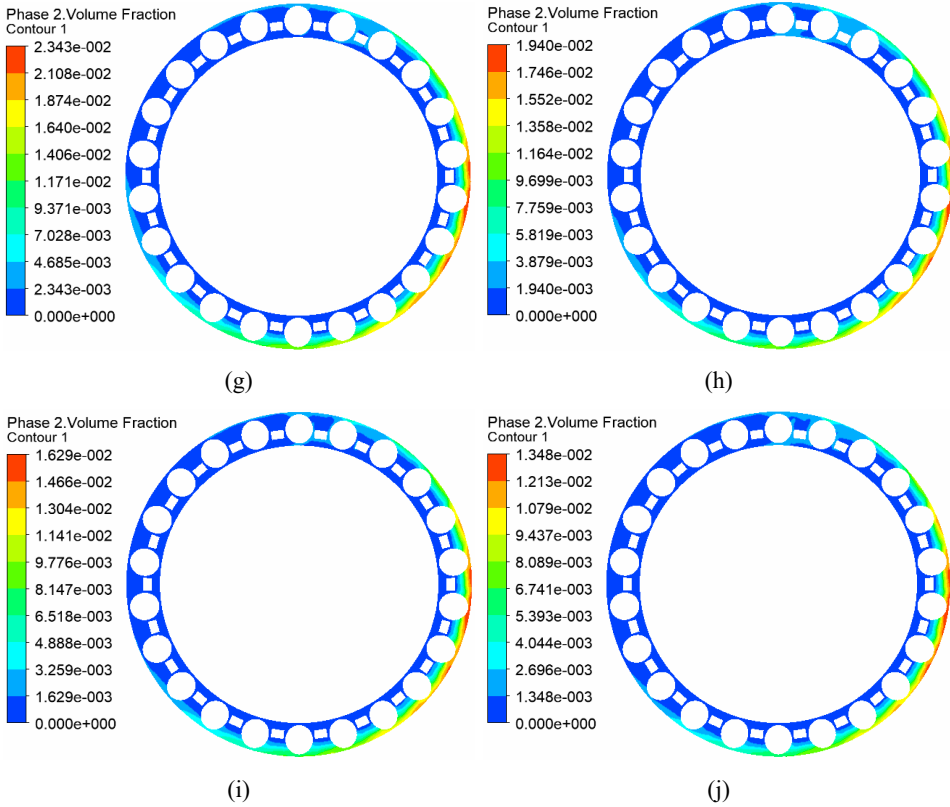


**Table 1** Division of discrete nodes of oil mass in the loss of lubrication process.

<i>Node</i>	<i>1</i>	<i>2</i>	<i>3</i>	<i>4</i>
Oil mass (kg/s)	0.02	0.016	0.0126	0.01
Node	5	6	7	8
Oil mass (kg/s)	0.008	0.0063	0.005	0.004
Node	9	10	11	
Oil mass (kg/s)	0.0032	0.0025	0.002	

*5.2 Change in lubricating oil at the cross section of the large roller*

From the simulation results of the loss of lubrication process in Figure 13, it can be seen that during the process of reducing the inlet oil volume from 0.02 to 0.005 kg/s, the volume fraction of lubricating oil at the section of the large roller continues to decrease, and there is no obvious point of exhaustion. However, when it decreases to 0.004 kg/s, an area with an oil volume fraction of zero appears in the section of the large roller, and an obvious point of oil depletion appears on the walls of the inner and outer rings at the

same time. In addition, the lubricating oil between the roller and the inner ring is lost quickly during the loss of lubrication process. According to the analysis in the second section, this is because the oil droplets are more likely to adhere to the outer ring wall surface. The bearing ribs are set on the outer ring, and the lubricating oil is not blocked when it is released from the bearing cavity along the inner ring wall, which intensifies its loss on the inner ring wall during this process.

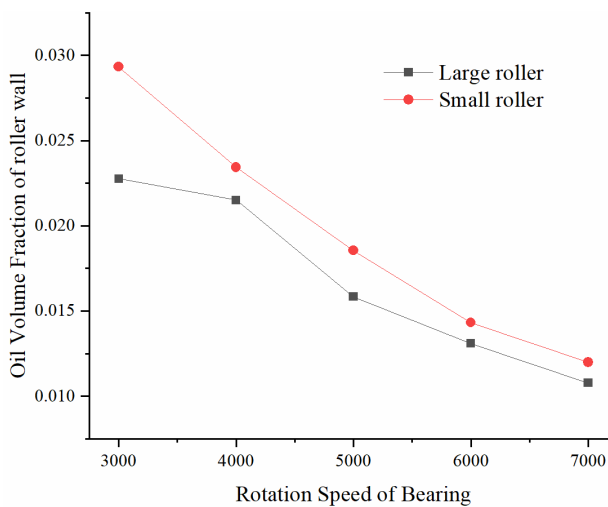
## 6 Optimisation of design parameters of asymmetric double-row tapered roller bearings

In the loss of lubrication process and normal lubrication, the lubricating oil distribution inside the bearing is similar. Therefore, a design parameter analysis under the fully lubricated state was carried out, including the input speed and structural parameters (the number of rollers). The influence of the number of rollers on the bearing lubricating oil distribution provided a reference for bearing structure design with good loss of lubrication characteristics.

### 6.1 Selection range of input speed

The control inlet oil mass was 0.02 kg/s, and the inner ring rotation speeds were 3,000, 4,000, 5,000, 6,000, and 7,000 r/min. The oil distribution is shown in Figure 14. It can be seen that the volume fraction of oil on the wall of the small roller is always higher than that of the wall of the large roller, and when the input speed increases, the oil volume fraction on the wall of the small and large rollers decreases. This is because the centrifugal force of the oil droplets also increases when the speed increases and bearing parts such as rollers and cages exert greater force on lubricating oil droplets, making oil storage more difficult.

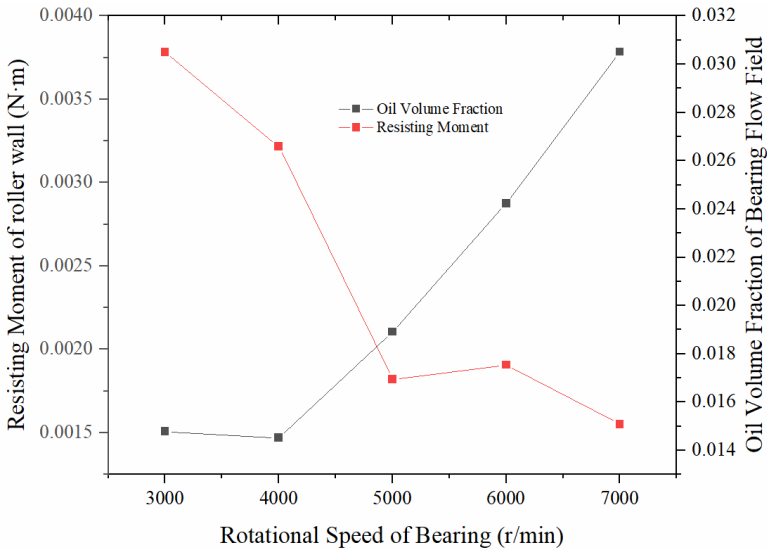
**Figure 14** Influence of inner ring rotation speed (see online version for colours)



As shown in Figure 15, when the input speed is 3,000–5,000 r/min, the oil volume fraction in the bearing basin decreases rapidly when the speed increases; when the input speed is 5,000–7,000 r/min, the oil volume fraction first increases and then decreases as the speed increases. When the input speed increases, the volume fraction of the oil on the roller wall surface decreases and affects the roller lubrication. At the same time, when the volume fraction of the oil in the watershed decreases, the heat carried away by the oil also decreases. However, if the volume fraction of the oil is too high, it will cause an increased oil-stirring power loss.

Therefore, when determining the input speed, factors such as lubrication, heat dissipation, and bearing power loss should be comprehensively considered. The relationship between the roller resistance torque and input speed is shown in Figure 15. According to this analysis, the recommended input speed range is 4,000–5,000 r/min, and the best input speed is approximately 4,000 r/min. This number is similar to the recommended rotating speed range for the research of Lu et al. (2020). At this speed, the oil volume fraction on the bearing wall is high, and the bearing cavity has more oil to remove the bearing heat. Moreover, the resistance moment of the bearing roller is the smallest.

**Figure 15** Relationship between the roller resistance torque and input speed (see online version for colours)

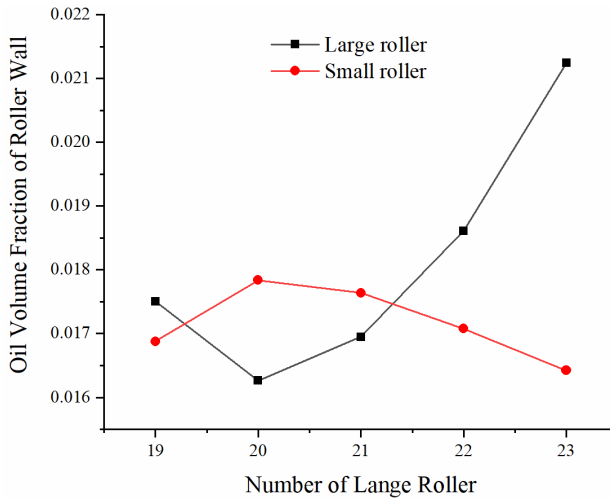


## 6.2 Determination of the number of rollers

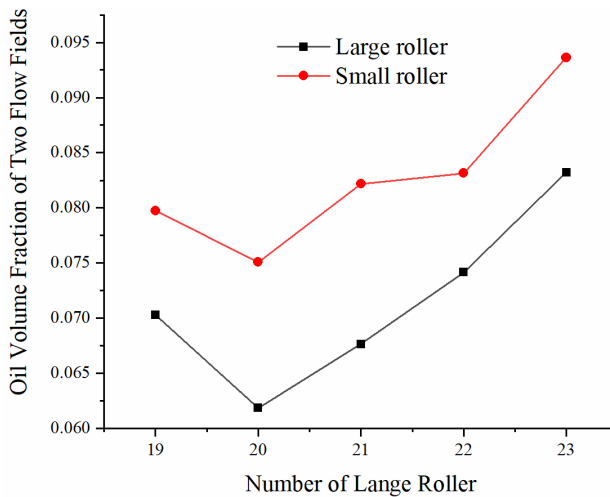
The number of small rollers was set to 22, the inlet oil volume was set to 0.02 kg/s, the number of large rollers was varied, and the change in the volume fraction of lubricating oil in the bearing basin was observed, as shown in Figure 16. It can be seen that with a constant number of small rollers and an increase in the number of large rollers, the oil volume fraction on the wall surface of the large roller decreases first and then increases, and the oil volume fraction on the wall surface of the small roller first increases and then decreases. When the number of large rollers is greater than 22, the rate of change in the

oil volume fraction on the wall surface of the large and small rollers increases. However, the volume fraction of lubricating oil inside the small and large roller bearings first decreases and then increases.

**Figure 16** Influence of the number of large rollers, (a) oil distribution change at the roller wall, (b) oil distribution change at the two-flow field (see online version for colours)



(a)

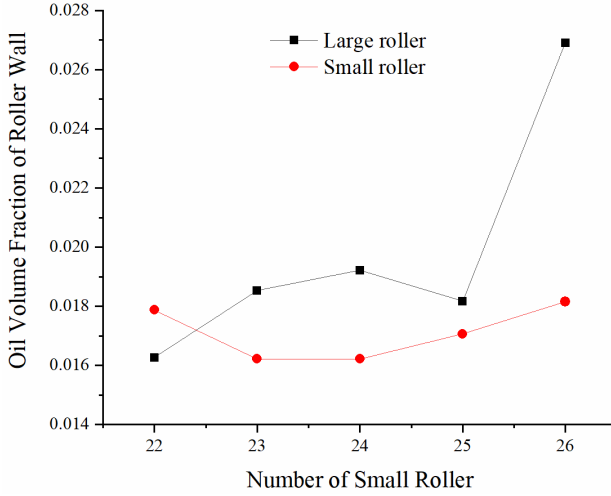


(b)

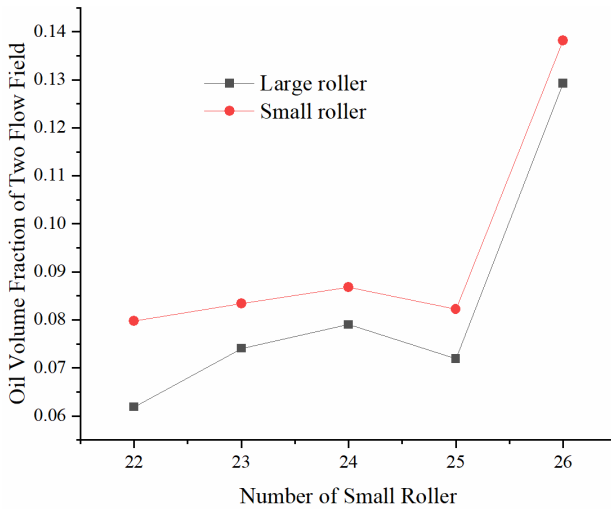
Similarly, the number of large rollers in the bearing was set to 20, the inlet oil volume was set to 0.02 kg/s, the number of small rollers was varied, and the change in the volume fraction of lubricating oil in the bearing basin was observed, as shown in Figure 17. The number of large rollers remains unchanged, whereas the number of small rollers increases. The volume fraction of the oil on the wall of the small rollers first decreased and then increased. The volume fraction of oil on the wall of the large rollers shows an

overall upward trend and decreases slightly when the number of small rollers is 25. The volume fraction of lubricating oil in the rotation area of the bearing rollers increases with an increase in the number of small rollers. When the number of small rollers is 25, the volume fraction on the bearing decreases slightly, and when the number of rollers exceeds 25, it decreases quickly.

**Figure 17** Influence of the number of small rollers, (a) oil distribution change at the roller wall, (b) oil distribution change at the two-flow field (see online version for colours)



(a)



(b)

According to the position of the bearing in the helicopter reducer shown in Figure 2, it can be seen that the large roller end bears a larger load and an appropriate increase in the number of rollers can effectively improve the bearing capacity of the rollers. However, changes in the number of large and small rollers affect the distribution of the oil-gas

two-phase flow inside the bearing. As the number of large and small rollers increase, the volume fraction of the lubricating oil inside the bearing generally increases. The volume fraction of lubricating oil on the roller wall affects the lubrication of the rollers, while the volume fraction of lubricating oil inside the bearing affects the power loss. If the number of rollers is too high, the strength of the cage cannot be guaranteed. Therefore, it is recommended that the number of small rollers be within 22–25 and the number of large rollers be within 20–22.

## 7 Prediction of the volume fraction of lubricating oil inside the bearing

### 7.1 Numerical fitting of the volume fraction of lubricating oil inside the bearing

To guide the design and selection of medium-reduction bearings, the change of the volume fraction of lubricating oil inside the bearing according to the number of rollers and the amount of inlet oil is numerically fitted. MATLAB was used for the fitting, and a suitable fitting model was selected to minimise the error after fitting. The fitting result is shown in equation (4). After comparison, it was found that the volume fraction of the lubricating oil in the bearing cavity was significantly affected by the amount of inlet oil. The weight of the inlet oil volume in the fitting was appropriately increased, and the result is shown in equation (5).

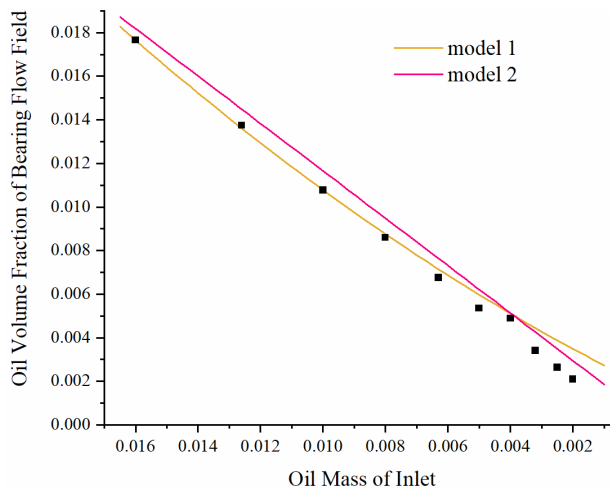
$$\alpha = -2.014 + 12.09 \sin\left(0.01639\pi \frac{Z_2 f_{in}}{Z_1}\right) - 2.012 e^{-(2.88 f_{in})^2} \quad (4)$$

$$\alpha = -0.09557 + 0.3066 \sin\left(0.9903\pi \frac{Z_2 f_{in}}{Z_1}\right) - 0.09744 e^{-(0.9435 f_{in})^2} \quad (5)$$

where  $Z_1$  is the number of large rollers,  $Z_2$  is the number of small rollers, and  $f_{in}$  is the inlet oil mass.

### 7.2 Verification of the fitting results

To verify the accuracy of the fitting results, the bearing was modelled and calculated. The number of large and small rollers in the new model was set to 21 and 24, respectively. The volume fraction of the lubricating oil in the bearing cavity at each loss of lubrication process node was plotted. The fitting results of models 1 [equation (4)] and 2 [equation (5)] are shown in Figure 18. Model 1 is more accurate than model 2 in predicting the volume fraction of lubricating oil in the bearing cavity when the amount of inlet oil is sufficient. However, model 2 always maintains a certain prediction accuracy during the entire the loss of lubrication process; therefore, it is used in subsequent calculations. When model 2 is used to predict the change in the volume fraction of lubricating oil in the bearing cavity during the loss of lubrication process, the accuracy is always less than 20%, and the maximum error is 16.13%.

**Figure 18** Fitting model verification (see online version for colours)

## 8 Conclusions

The volume fraction of the lubricating oil on the bearing roller wall surface decreased as the input speed of the bearing increased; however, the volume fraction of the lubricating oil in the bearing cavity first decreased, then increased, and then decreased again as the input speed of the bearing increased to produce the best operational performance. Considering the lubrication and power consumption characteristics of the bearing, it is recommended that the input speed of the bearing be within 4,000–5,000 r/min.

The bearing size and number of rollers influence the oil-gas two-phase flow in the bearing cavity. Increasing the number of rollers, the bearing load state will improve, but it may have an adverse impact on the lubrication. The number of large rollers in the bearing should not exceed 22, while the number of small rollers should not exceed 25.

Two mathematical models were used for predicting the change of the volume fraction of lubricating oil in the bearing during the loss of lubrication process. The forecast accuracy of the model can be improved if increase the weight of the inlet oil volume in the mathematical model.

Future, the temperature characteristics of the bearing in the loss of lubrication situation can be analysed. Further, the dynamic characteristics of the bearing oil film in this process can be obtained based on the principle of elastohydrodynamic.

## References

- Bristol, A., Morvan, H.P. and Simmons, K.A. (2016) 'Evaluation of a volume of fluid CFD methodology for the oil film thickness estimation in an aero-engine bearing chamber', in: *Turbo Expo: Power for Land, Sea, and Air*, American Society for Mechanical Engineers, p.49712, V02CT39A007.
- Concli, F., Schaefer, C.T. and Bohnert, C. (2020) 'Innovative meshing strategies for bearing lubrication simulations', *Lubricants*, Vol. 8, No. 4, p.46.

- Crouchez-Pillot, A. and Morvan, H.P. (2014) 'CFD simulation of an aeroengine bearing chamber using an enhanced volume of fluid (VOF) method: an evaluation using adaptive meshing', in *Turbo Expo: Power for Land, Sea, and Air*, American Society for Mechanical Engineers, p.45738, V05CT16A033.
- Guo, K., Yuan, S.H. and Shao, Z.T. (2012) 'Study on oil-air two-phase flow inside the high-speed bearing cavity with jet lubrication', *Transactions of Beijing Institute of Technology*, Vol. 32, No. 10, pp.1022–1025.
- Hu, J., Wu, W., Wu, M. and Yuan, S. (2014) 'Numerical investigation of the air-oil two-phase flow inside an oil-jet lubricated ball bearing', *International Journal of Heat and Mass Transfer*, Vol. 68, pp.85–93.
- Li, Y., Yang, Z., Chen, F. and Zhao, J. (2018) Effect of air inlet flow rate on flow uniformity under oil-air lubrication', *Industrial Lubrication and Tribology*, Vol. 70, pp.282–289.
- Liang, H., Zhang, Y. and Wang, W.Z. (2020) Experimental observation and investigation of oil distribution and replenishment in a rolling bearing model', *Tribology*, Vol. 40, No. 4, pp.450–456.
- Liu, H.B., Liu, G.P., Li, Y.B. and Wang, L. (2018) 'Numerical investigation of two-phase air/oil flow in high-speed angular-contact ball bearing chamber', *Journal of Aerospace Power*, Vol. 33, No. 5, pp.1103–1111.
- Lu, F.X., Wang, M., Wang, C.L., Zhu, R.P. and Zhu, W.L. (2020) 'Analysis and optimization method for flow field of intermediate gearbox splash lubrication in helicopters', *Acta Aeronautica et Astronautica Sinica*, Vol. 41, No. 11, pp.123659–123659.
- Peterson, W., Russell, T., Sadeghi, F., Berhan, M.T., Stacke, L.E. and Ståhl, J. (2021) 'A CFD investigation of lubricant flow in deep groove ball bearings', *Tribology International*, Vol. 154, p.106735.
- Raju, K.S., Veettil, M.P., Ray, S. and Shi, F. (2013) 'Needle roller bearing lubricant flow CFD simulations', in *2013 Symposium on International Automotive Technology*, SIAT Campus Pune, pp.25369–25373.
- Wenwei, A., Hua, S. and Guoding, C. (2009) 'Numerical simulation of gas and liquid flow in a bearing chamber', *Mechanical Science and Technology for Aerospace Engineering*, Vol. 28, No. 8, pp.1064–1067.
- Wu, W., Hu, C., Hu, J. and Yuan, S. (2016a) 'Jet cooling for rolling bearings: flow visualization and temperature distribution', *Applied Thermal Engineering*, Vol. 105, pp.217–224.
- Wu, W., Hu, J., Yuan, S. and Hu, C. (2016b) 'Numerical and experimental investigation of the stratified air-oil flow inside ball bearings', *International Journal of Heat and Mass Transfer*, Vol. 103, pp.619–626.
- Yan, K., Wang, Y., Zhu, Y. and Hong, J. (2017) 'Investigation on the effect of sealing condition on the internal flow pattern of high-speed ball bearing', *Tribology International*, Vol. 105, pp.85–93.
- Yan, K., Wang, Y., Zhu, Y., Hong, J. and Zhai, Q. (2016a) 'Investigation on heat dissipation characteristic of ball bearing cage and inside cavity at ultra high rotation speed', *Tribology International*, Vol. 93, pp.470–481.
- Yan, K., Zhang, J., Hong, J., Wang, Y. and Zhu, Y. (2016b) Structural optimization of lubrication device for high speed angular contact ball bearing based on internal fluid flow analysis. *International Journal of Heat and Mass Transfer*, 95, 540–550.
- Zhai, Q., Yan, K., Zhang, Y., Hong, J. and Zhu, Y. (2014) 'Investigation of airflow pattern and heat transfer efficiency inside cavity of high-speed angular contact ball bearing', *Journal of Xi'an Jiaotong University*, Vol. 48, No. 12, pp.86–90.
- Zhang, R., Wei, C. and Wu, W. (2015) 'CFD investigation on the influence of jet velocity of oil-jet lubricated ball bearing on the characteristics of lubrication flow field', in *2015 International Conference on Fluid Power and Mechatronics*, IEEE, pp.1324–1328.
- Zhang, Y. (2018) *Investigation on Lubrication Performances and Thermal Characteristics of a Tapered Roller Bearing*, Chongqing University.

## **Notes**

- 1 Relevance to design practice – it provides a good reference for loss of lubrication characteristics for bearing structure design. Provide reference for selection of bearings in the same working environment.